Impact of 3D Surface Scanning Protocols on the Os Coxae Digital Data: Implications for Sex and Age-at-death Assessment

Anežka Kotěrová, Vlastimil Králík, Rebeka Rmoutilová, Lukáš Friedl, Pavel Růžička, Jana Velemínská, François Marchal, Jaroslav Brůžek

Impact of 3D Surface Scanning Protocols on the *Os Coxae* Digital Data: Implications for Sex and Age-at-death Assessment

Anežka Kotěrová [a], Vlastimil Králík [b], Rebeka Rmoutilová [a,c], Lukáš Friedl [d,e], Pavel Růžička [b], Jana Velemínská [a], François Marchal [f], Jaroslav Brůžek [a,c]

[a] Department of Anthropology and Human Genetics, Faculty of Science, Charles University, Viničná 7, Prague, 128 43, Czech Republic

[b] Department of Mechanics, Biomechanics and Mechatronics, Faculty of Mechanical Engineering, CTU in Prague, Technická 4, Prague, 166 07, Czech Republic

[c] Laboratoire PACEA, UMR 5199, CNRS, Université Bordeaux, CS 50023, Pessac,33615, France

[d] Department of Anthropology, University of West Bohemia, Plzeň, 30614, Czech Republic

[e] Interdisciplinary Center for Archaeology and Evolution of Human Behaviour (ICArEHB), Faculdade das Ciências Humanas e Sociais, Universidade do Algarve, Campus Gambelas, 8005-139, Faro, Portugal

[f] UMR 7268 ADES, Aix-Marseille University, EFS, CNRS, Faculté de Médecine Secteur Nord, 13344 Marseille Cedex 15, France

Corresponding author

Anežka Kotěrová

Email:
koterova.a@seznam.cz
Address :
Department of Anthropology and Human Genetics, Charles University
Viničná 7, Prague 2
128 43, Czech Republic

Abstract

The 3D imaging technologies became of paramount importance for example in disciplines such as forensic anthropology and bioarchaeology where they are being used more and more frequently. There is a number of new possibilities that they offer, for instance an easier and faster sharing of data among institutions, a possibility of permanent documentation, or new opportunities of data analysis. An important requirement, however, is whether the data obtained from different scanning devices are comparable and whether the possible varying outputs could affect further analyses, such as estimation of the biological profile. Therefore, we aimed to investigate two important questions: (1) whether 3D models acquired by two different scanning technologies (structured light and laser) are comparable and (2) whether the scanning equipment has an effect on the anthropological analyses, such as age-at-death estimation and sex assessment.

3D models of *ossa coxa* (n=29) were acquired by laser (NextEngine) and structured light (HP 3D Structured Light Scanner PRO 2) scanners. Resulting 3D models from both scanners were subjected to age-at-death analyses (via quantitative method of Stoyanova et al., 2017) and sex analyses (via Diagnose Sexuelle Probabiliste 2 of Brůžek et al., 2017). Furthermore, high quality scans of small sample (n=5) of pubic symphyseal surface with RedLux Profiler device were acquired as reference surfaces to which the outputs from both scanners were compared. Small deviations between surfaces were more evident in more rugged surfaces (in areas of depression and protrusion). Even though small differences from the reference surfaces were found they did not have significant effect on age and sex estimates. It never resulted in opposite sex assignment and no significant differences were observed between age estimates (with the exception of TPS/BE model).

Keywords

Laser Scanning; Structured Light Technology; RedLux Profiler; Biological Profile; Age and Sex Estimation; *Os Coxae*

1. Introduction

The 3D imaging technologies, i.e. surface scanning (both, laser and structured light), as well as computed tomography (CT) scanners and micro-CT scanners became widely used in anatomical research over the last few years [1]. All of these devices enable to obtain 3D models of desired objects. Surface scanning contrary to CT scanning offers several practical advantages, for instance higher portability of most devices, texture capture options, low cost, and rapid post-processing. Furthermore, they can be operated without certification since there is no radiation involved during

the scanning process [2–4]. On the other hand, internal structures remain hidden [4]. Scanning technologies based on visible light have spread to many different disciplines: e.g. to forensic science [5,6], anthropology and paleoanthropology [2–4,7], anatomy and morphology [8–11], and paleontology and archaeology [8,12,13]. They allowed for new applications and brought additional advantages. It is now possible, for instance, to create and archive digital copies of skeletal remains as 3D models in the virtual environment. Such digital osteological collections are invaluable for researchers for several reasons. First, they represent a possibility of permanent storage or documentation and conservation of bones, which are then accessible even though the real specimen is no longer available or does not exist anymore. Virtual storage can serve not only as a repository but also enables easier and faster sharing of data among researchers and institutions (e.g. [1,3,4,8,12,14,15]). The reduced need for physical manipulation with skeletal material is certainly a great advantage [15] since the preservation of dry bones varies as they are constantly being used for scientific purposes [16]. Virtual models could be used for teaching and research, as well as for 3D printing which can be used for exhibition purposes [10,17,18] or as demonstrative evidence in court [19,20]. Last but not least, digital technologies enable us to virtually reconstruct damaged skeletal material, e.g. incompletely preserved fossil remains [21–23].

Traditional methods of biological profile estimation which use morphometric or visual approach are usually used for defining the biological profile of an individual in bioarchaeology as well as in forensic anthropology (e.g. [24,25]). However, virtual bone models have become of paramount importance and are commonly used for instance to measure metric variables in order to estimate sex [26,27]. The consistency between dimensions taken directly from dry bones and from their virtual representations [27–30] and even from their printed replicas [19] has been proven repeatedly. Sex and stature estimates via linear measurements taken from virtual data obtained with two different laser scanners showed only a very small deviation from traditionally obtained data in one recent study [31]. Moreover, bones in virtual environment can undergo analyses that cannot be performed on dry bones, e.g. quantitative analyses of surface with the use of geometric morphometric.

For example, the geometric morphometric tools are used for sex estimation [32–34] and ancestry assessment [35,36]. To estimate age-at-death, the pelvic articulations (the pubic symphysis, the auricular surface, and the acetabulum) are often used since their surfaces undergo changes with aging and recently, these surfaces have begun to be evaluated quantitatively [37–41]. Such analyses tend to be more objective than traditional visual methods based on scoring as they allow for the evaluation of morphological variation of the skeletal material independent of the human eye and experience of the researcher [17].

Villa et al. [42] raised an important question whether the results of surface quantification used for age estimation from different laser scanners are comparable. The precision and repeatability of measurements among different scanning devices are necessary in order to ensure the reliability of biological profile estimation methods. We extended this question to another parameter of biological profile - sex estimation (besides age estimation) and, in contrast to the original study where only laser scanners were used, both, laser and structured light, scanners were compared.

The aims of the present study are twofold. The first is to compare 3D models of *os coxae* made by two different surface scanners (NextEngine laser scanner and HP 3D Structured Light Scanner Pro S2) with a reference sample derived from RedLux Profiler device. Second, we aimed at assessing whether the scanning equipment has an effect on the age-at-death estimation (via quantitative method of Stoyanova et al., 2017) and sex assessment (via DSP2 - Diagnose Sexuelle Probabiliste of Brůžek et al., 2017).

2. Material

The skeletal sample used in the present study originates from the cemetery of the 2nd church in Mikulčice settlement (9th–10th century AD), south Moravia, Czech Republic. This sample represents a medieval population of central Europe that belonged to the Great Moravian Empire [43]. We used 18 adult individuals, of which 11 had well preserved *ossa coxa* on both sides and seven individuals who only had left or right bone well preserved. Altogether, 29 *ossa coxa* were used in the present study. Only individuals with well-preserved articular surfaces (pubic symphysis and auricular surface) were selected. Even if we do not know the real age and sex of individuals, we can compare the resulting estimates derived from surface models digitized with different scanning technologies (HP 3D SLS, NextEngine and RedLux) with each other.

3. Methods

3.1.Digitization of skeletal material

A small sample of pubic symphyses (n=5) was digitized with the use of RedLux Profiler contactless metrology device (RedLux Ltd., Southampton, UK) [44,45]. Samples were selected to include both smooth and significantly wrinkled symphyses. The scanned surface of key areas was utilized as reference surface to compare the resolution and quality of scans obtained by commonly used scanners. The whole surface of *os coxae* (n=29) was then digitized with two different scanning devices: the NextEngine 3D scanner Ultra HD and HP 3D Structured Light Scanner PRO S2. The

scanning process as well as post-processing procedures with all three scanners are described in the following sections.

3.1.1. RedLux

The pubic symphyses of five selected *ossa coxa* were digitized using the RedLux profiler. The RedLux profiler device is designed for very precise surface measurements using a confocal sensor. Due to limited space capacity because of technical arrangement of the measuring device, physical casts of these five pubic symphyses needed to be obtained. As a casting material, the two-component Addition Cure Molding Rubber, known under the trade designation MM242R [46], was used. This material shows negligible volumetric change (linear shrinkage of 0.09%) and excellent quality and accuracy of surface reconstruction. It is also necessary to ensure thorough venting, using a desiccator and the vacuum pump that any air bubbles could not affect the volumetric change. Venting was carried out for min. of 10 minutes at 150 mbar vacuum. The resulting symphyseal cast for one selected sample is shown in Fig. 1.

[Figure 1, insert here]

The casts were scanned using a highly accurate RedLux profiler device. The instrument was equipped with two high-precision movable linear and two rotary axes. The rotary stages carry the sample and the linear stages carry the sensor. With this sensor, the lens error commonly known as chromatic aberration is used to measure the distance to an object. By combining the sensor signal with the knowledge of the exact position of all 4 stages, 3D representation of the surface can be created. The instrument has the capability to measure the entire surface in a single procedure. The accuracy of the resulting point cloud is given by the resolution of 2 linear axes, resolution of the two rotational axes and the resolution of the probe. The resolution of each linear axis is 100 nm, the resolution of each rotary axis is 10 arc second and the resolution of the probe is 20 nm. Detailed description of the RedLux profiler device can be found in [47]. The arrangement of the measuring device is shown in Fig. 2.

[Figure 2, insert here]

Since the measurement of a surface by RedLux profiler is a free-form surface measurement task, it is important to scan the surface with a sufficiently dense point cloud to capture the real scanned surface with all its irregularities. Throughout all of the performed measurements, the point cloud density was 540 individual points per one rotation of the measured sample in vertical plane and

within every single rotation, the measured sample was shifted approximately by 0.1 mm in the horizontal plane. More than 120,000 points were obtained for each sample using RedLux profiler device. The resulting point cloud for the selected sample is shown in Fig. 3.

[Figure 3, insert here]

As it is shown in the Fig. 3, the point coverage on the sample surface is irregular due to the used scanning method. For subsequent comparison with HP 3D Structured Light Scanner Pro S2 and NextEngine laser scanner, it was necessary to get a regular network of points. First, the co-ordinate data collected from the RedLux profiler were interpolated using Matlab's function *scatteredInterpolant* (The Mathworks, Inc.). This function is included in the basic Matlab package and performs interpolation on 3D set of points that have no structure among their relative locations (scattered data set).

Interpolation step Δ = 0.025 mm and 'natural' interpolation method was chosen for both directions and it specifies the density of the net. Detailed description of this function can be found in the software Matlab [48]. Mesh representation of the surface is shown in Fig. 3.

3.1.2. NextEngine and HP 3D Structured Light Scanner PRO S2

The whole sample of *ossa coxa* was digitized by two different surface scanners. The laser scanner NextEngine 3D scanner Ultra HD and HP 3D Structured Light Scanner PRO S2 (previously known as DAVID SLS 2) with maximum resolution of 0.1 mm and 0.05 mm, respectively, were utilized. These two scanners represent different scanning technologies: laser and structured light technology. Since the aim of the present study is to compare the resulting 3D models from different surface scanners in terms of their surface representation and their possible impact on sex and age estimation, 3D models were created under the optimal conditions for the particular scanner.

The entire surface of *os coxae* was scanned to facilitate creation of the osteological collection, however only partial surfaces were used for some of the analyses in this study. The scanning process, as well as the post-processing (aligning multiple scans of each bone together to form a final polygonal mesh) was performed in the integrated software of each scanner (ScanStudio HD and David LaserScanner v.3.10.4, respectively). In the case of HP 3D Structured Light Scanner PRO S2 (hereinafter HP 3D SLS) the calibration was done with the 120 mm pattern that is ideal for objects of similar size to an *os coxae*. The scanning procedure was performed against black background and the scanned *ossa coxa* were manually rotated from both, the ventral and dorsal sides to create a solid

model. In the case of NextEngine scanner, a dedicated rotational device was used to fix the bone and rotate it in front of the scanner so that each individual scan overlaps with the previous and the next one. Final scan was automatically assembled from these individual scans in the ScanStudio HD software. Each bone was attached to the device in two points, one along the iliac crest and one just in front of the ischial tuberosity. Both points were selected to minimize the areas where the laser beam does not reach and thus, to ensure that if there is a fraction of the surface to be reconstructed, such area is very small. These contact areas with the rotational device might have had approximately $1mm^2$ each.

The final 3D models were saved in the stl format. Each mesh had to be simplified (consistent simplification on 3 millions of faces) in order to facilitate the manipulation. Subsequently, 3D models from the NextEngine 3D scanner had to be scaled (in MeshLab software [49]) to obtain the same dimensions as the models from HP 3D SLS. The models of whole *ossa coxa* were used for sex estimation while the articular surfaces of pubic symphysis that we isolated from the rest of the bone (in MeshLab software) served as input data for age-at-death estimation.

3.2.Comparison of resulting 3D surfaces

Once the mesh representation of the pubic symphyseal surface was created, it became important to calculate the distribution of deviations between the actual and reference surfaces. Both surfaces were overlapped using the *local best fit* feature implemented in the commercially available software GOM Inspect [50]. The function minimizes differences (square error) through all of the used points and the software tries to align the point sets so the differences are zero or as close to zero as possible. Resulting deviations were assessed with descriptive statistics (mean, standard deviation, median, and interquartile range) for all samples.

3.3.Biological profile assessment

3.3.1. Sex estimation

Linear dimensions derived from 3D surface models taken with two different scanners and dimensions taken directly from dry *ossa coxa* served as the input data for the DSP2 (Diagnose Sexuelle Probabiliste 2) sex determination method [51,52]. The DSP2 method is based on linear discriminant analysis and posterior probabilities. The output of this sex determination tool is the probability of being male or female (sex is determined if the posterior probability is ≥ 0.95). Ten variables (or the number that could be measured for a given bone depending on its preservation, but at least four) were measured according to their definitions (Table 1) described in the software interface. The variables were first measured on dry bones with appropriate measuring instruments (sliding caliper,

friction divider, and pelvimeter). Second, measurements on 3D models were carried out in the Morphome3cs software [53] in the virtual environment. Additionally, ten randomly chosen *ossa coxa* were measured twice over a period of four weeks (for all three types of acquisitions) for intra-observer error. All the measurements were taken by two researchers (AK and RR) both trained in pelvic osteometry with approximately the same experience. Apart from the intra-observer error calculated for linear variables, the inter-observer error between two equally trained observers was calculated as well.

[Table 1, insert here]

To verify the accuracy of measured dimensions within each type of data taken by one observer (intra-observer error) the technical error of measurement (TEM) and the relative TEM (*r*TEM) expressed as a percentage were calculated. Both statistical characteristics are commonly used to evaluate intra-observer precision [26,29,54–56]. The inter-observer error was computed for measurements taken on dry bones and on 3D models acquired with both scanners. A paired t-test was applied to assess whether significant differences between the two observers exist.

3.3.2. Age-at-death estimation

Age-at-death of our sample was estimated with the use of a recent computational method of Stoyanova et al. [39,40]. This fully quantitative evaluation of pubic symphyseal surfaces is based on mathematical evaluation of the flatness of the surface, the curvature of ventral margin of pubic symphysis and their combination. The flatness of the surface captures the TPS/BE (Thin Plate Spline/Bending Energy) analysis and SAH-Score (described in detail in [38]). The last computational method captures the curvature of ventral margin (VC) of pubic symphysis. These analyses are incorporated into the "forAge" software. Detailed description can be found in the original study [40].
The isolated articular surfaces of the pubic symphyses were simplified to 15,000 faces and saved in the ply format before loading to the forAge software to estimate the age-at-death. All the isolated pubic symphyseal surfaces (n=29) from the NextEngine, the HP 3D SLS, and the small sample (n=5) from RedLux were subjected to this quantitative analysis. The 3D models digitized with HP 3D SLS and NextEngine were compared using paired t-test. The small sample (n = 5) of pubic bones digitized with RedLux was also compared with the other samples. Differences within corresponding individuals between RedLux and HP 3D SLS and NextEngine respectively were evaluated with a paired one-sample t-test.

4. Results

4.1.Comparison of resulting 3D surfaces

Examples of three isolated pubic symphyseal surfaces digitized with the three scanning devices are shown in Fig. 4.

[Figure 4, insert here]

Visualization has been made in the form of color-coded maps of scatters of deviations between the reference and compared scans. This comparison was performed for all 5 selected specimens, both for HP 3D Structured Light Scanner Pro S2 and NextEngine laser scanner. The color scale bar on the map of deviations shows both positive and negative dimensional changes. The positive scale (red color) means that the compared surface is above the reference one and the negative scale (blue color) indicate that the compared surface is below the reference one. Gray color refers to the surface where no data were available from compared scanners (HP 3D SLS and NextEngine).

Example of color-coded maps for selected specimens are shown in Fig. 5. It can be seen that the largest and the smallest deviations from the reference surface are in the area of depressions or protrusions. This is more evident on specimens with more rugged surface (e.g. specimen no. 390). It shows that scans acquired by HP 3D SLS and NextEngine are smoothed out and do not capture as much detail as the reference surface obtained with RedLux profiler. This is due to the resolution of a particular scanning technology.

[Figure 5, insert here]

Descriptive statistics of the resulting deviations are summarized in Table 2. The graphical comparison of the examined scanners is in Fig. 6 for all samples in the form of box plots. The deviations from the reference surface were slightly larger for the NextEngine than for the HP 3D SLS. In the case of NextEngine scanner, the interquartile range is higher for all samples and the standard deviation is higher as well, except for sample no. 383. Contrary to the NextEngine, there are more places where no data are available in scans from the HP 3D SLS, particularly in major depressions. From Table 2 and Fig. 6, it can also be seen that the value of the percentage difference of *IQR* is related to the degree of wrinkling of the surface. The percentage difference of *IQR* is significantly higher in samples which are more wrinkled, such as the sample no. 390 where a relatively large lateral wrinkling is evident (Fig. 5).

[Figure 6, insert here]

[Table 2, insert here]

4.2.Sex estimation

For manual DSP method as well as for virtual DSP performed on both 3D models (HP 3D SLS and NextEngine) comparisons of estimated sexes (and agreement) between two observers were performed. The results of agreement in estimating male, female, and undetermined sex (N/A) of two researchers are shown in Tables 3 to 5. Some differences between observers were found, however opposite sex was never assigned to the same individual (rather, such individual was assigned as N/A).

[Tables 3 to 5, insert here]

4.2.1. Intra and inter-observer error of measurements

Results of intra-observer error are presented in Table 6. With measurements on dry bones, average TEM values were 0.80 mm and 0.62 mm respectively. TEM values for dry bones ranged between 0.32 and 1.35 mm with *r*TEM 0.35% – 3.09% for the first researcher and for the second researcher from 0.45 to 1.01 mm, *r*TEM 0.20% – 2.07%. The lowest average TEM values were reached by both researchers coincidently in the case of HP 3D SLS (0.62 and 0.56 mm respectively). The intra-observer error of the researcher 1 ranged between 0.35 and 1.24 mm for all ten dimensions and the *r*TEM ranged between 0.21% and 2.85%, and for researcher 2 between 0.24 and 0.88 mm with *r*TEM from 0.19% to 2.22%. The average intra-observer error for NextEngine was very similar to previous results (0.72 mm and 0.57 mm respectively). The error for the first researcher was between 0.26 and 1.38 mm, *r*TEM 0.20% – 2.36% and TEM of researcher 2 ranged from 0.12 to 1.19 mm, with *r*TEM of 0.07% – 1.95%.

[Table 6, insert here]

The results of inter-observer error for variables measured directly on dry bones, on 3D models digitized with HP 3D SLS, and NextEngine respectively, are shown in Table 7. Significant differences between the two researchers when dry bones were measured have been found for IIMT, ISMM, SCOX, SS, and VEAC). DSP variables measured on 3D models from HP 3D SLS scanner were statistically different between the two researchers in IIMT, ISMM, SCOX, SS, SIS, and VEAC. Inter-observer differences were also found for 3D measurements derived from NextEngine, namely for PUM, DCOX, SS, and VEAC.

[Table 7, insert here]

4.3.Age estimation

A paired t-test was applied to reveal potential differences between estimated ages derived from the 3D models of the isolated pubic symphyses from the NextEngine and the HP 3D SLS. The results are provided in Table 8. Differences in estimated ages were not statistically significant. The only exception was the TPS/BE regression model. Thus, the null hypothesis was not rejected for any of the models, except for TPS/BE model. These results can be interpreted as a negligible effect of scanning technologies on age estimation in this study. The sample of isolated pubic symphyseal surfaces derived from the RedLux Profiler (n=5) was also subjected to the age-at-death analysis. We did detect differences between HP 3D SLS and RedLux for SAH model, and between NextEngine and Redlux in SAH and SAH+VC model. The null hypothesis was not rejected in all other cases (see Table 9).

[Tables 8 and 9, insert here]

5. Discussion

Scanning – problem of compatibility

Many researchers travel around the world and study osteological collections to design new methods or to validate already existing ones. Scanning technologies are already used in biological and forensic anthropology and became of paramount importance (e.g. [4,7,57]). One of the greatest benefits is a digital storage and sharing of osteological material. The material can come to researchers or it can be publicly available under certain conditions. However, research institutions are equipped with different scanning devices that may produce varying outputs.

Therefore, it is necessary to verify that the outputs from different devices are comparable to each other (and under what settings) and that they do not affect further analyses such as the estimation of the biological profile. The comparability of outputs from different devices is especially important in age-at-death estimation since minor changes on joint surface may influence the final estimate significantly. However, the consistency of outputs from different devices for biological profile estimation needs to be tested. This has not yet been sufficiently explored, except for a few exceptions, such as the aforementioned study of Villa et al. [42].

To test the effect of scanning device on forensic methods of biological profile estimation we chose the sex and age-at-death estimation. For sexing, the method called DSP is well established, and its reliability has been proven and guarantees objectivity (e.g. [26,27,58,59]). The forAge software is one

of the few age estimation approaches using mathematical quantification of bone surface that has been published so far. Repeatability of the method was tested with excellent results [60] and its use is suitable for individuals under 40 years of age [61].

The advantages and disadvantages of both scanners (NextEngine and HP 3D Structured Light Scanner PRO S2) and the technologies represented by them should be discussed to help future users assess them for their research goals. Both scanning technologies are used on skeletal material. However, laser scanning technology is generally preferred among anthropologists [17]. One of the most often used scanners is the NextEngine laser scanner (e.g. [7,10,38,62–64]) which was also used for a development of one method of age estimation that we tested in our study [39,40]. Although less attention has been paid to HP 3D SLS, its use is now on the rise. HP 3D SLS was used or tested in many studies on human or animal bones, as well as for other purposes [18,65–72]. Both tested scanners are commercially available, and they belong to the low-cost category of scanners (under $ 3,000), which makes them accessible to a great number of users. Moreover, the cost vs. performance ratio very often makes them the first choice. In terms of time needed to acquire and post-process scans, HP 3D SLS outperforms NextEngine scanner, mainly because the laser technology is more time consuming than other technologies [4,15]. Both scanners are characterized by high portability, and can be easily carried to various collections around the world. Also, both scanners are able to capture texture and provide 3D textured mesh as an output which is often a great benefit [7]. NextEngine as well as HP 3D SLS have, nonetheless, some limitations. Although laser and white light scanners are commonly used on skeletal material, they are limited in scanning dark and transparent objects or objects reflecting light (e.g. tooth enamel) [7,73]. Systems using blue light (e.g. HP 3D SLS) should reduce this limitation [7], however one of the authors (A.K.) who routinely operates with the HP 3D SLS has experienced similar issues (problems to capture very dark areas on objects). In case of HP 3D SLS, constant ambient light during scanning is recommended and a generally darker room is better suited for scanning.

It has to be emphasized that the quality of 3D models could be affected by post-processing. The simplification is often required to reduce file size, fasten data processing and manipulation with virtual data [4,74]. Even though in case of smoothing procedures, the positive or negative effect on mesh topology depends on algorithm used, decimation procedure always leads to loss of information, which affects mesh topology and measurements. With increasing the mesh triangle size, the accuracy of measurements is negatively affected [74,75]. The amount of decimation should be defined with regards to the type of objects and the purpose for which it will be used [4,74]. In the present paper, the only post-processing step performed was decimation, in order to enable for a

better manipulation since the whole *ossa coxa* were scanned. Simplification was applied to all models equally to enhance manipulation with minimum information lost. Other post-processing procedures (e.g hole filling, smoothing) were not performed to prevent the quality of the scan being negatively affected. Therefore, the dimensions in our study could not be affected by different post-processing procedures. However, it would be of great benefit for future studies if somebody tested how much simplified can the surface be without loosing too much information and getting inaccurate or imprecise estimates.

In our study, we worked with the assumption that different scanner operators or different scanning protocols do not affect the resulting 3D models and their geometric properties [75]. However, all the virtual data was acquired by experienced operators to ensure the consistency of scanned data. All the data was taken under the optimal conditions of each scanner. Since it is complicated to compare scanning devices among themselves, such an approach seemed the most reasonable to us. Moreover, it was also used in the study by Villa et al. [42].

Comparison of tested devices

Even the visual inspection of final 3D models revealed that Redlux scanner captures much more detail than the other two low-cost scanners.

Our results indicate that the NextEngine laser scanner has captured fewer details (it smoothed the surface the most and the loss of information was the largest) than HP 3D Structured Light Scanner when compared to reference scans from Redlux Profiler. Singh et al. [76] reported that structured light technology is more accurate in comparison to laser technology when used to calculate surface area and volume. Results of another study [15] indicate that structured light technology captured external structures better than other technologies (including laser technology). It should be noted here that these differences, as found in our study, are relatively small and their impact on further analyses (biological profile analyses) will be negligible**.** Our analyses of sex and age estimation confirm this notion.

Influence of different scanning device on the linear measurements and sex assessment

Both observers estimated sex of all individuals almost uniformly independently on the scanning technology. The intraobserver and interobserver errors of linear measurements were evaluated. According to Camison et al. [77] who divided *r*TEM values into five categories: <1% = excellent, 1–3.9% = very good, 4–6.9% = good, 7–9.9% = moderate, and >10% = poor, intraobserver error of both researchers in most cases fell into “excellent” category and the rest into “very good” category (the highest value reached 3.09%). Even though, our results of inter-observer error show some statistically significant differences between two observers, which may not be due to different

scanners, they have never led to the opposite classification. Here, our results could be interpreted in a similar way as in the study of Mullins and Albanesse [31], that even significant differences may not affect estimates and utility of this type of data. To our best knowledge, this is the first study testing the DSP method on virtual models acquired by surface scanners. Previously, the method was tested only on 3D models acquired with the CT scanning (e.g. [26,27,59]).

Effect of scanning device on delicate surface changes in the age-at-death estimation

Although the comparison of captured surfaces from both low-cost scanners showed slightly better outputs for the HP 3D SLS, almost no effect on quantitative methods of age estimation was detected (the only exception was TPS/BE model). We can conclude that other scanning technologies (at least structured light, here represented by the HP 3D SLS) can be used to estimate age using the method of Stoyanova et al. [39,40].

When compared to the outputs obtained with the Redlux, significant differences in one out of five models were found in case of HP 3D SLS and two out of five for the NextEngine. However, it was not assumed in our study that Redlux should be used to estimate age-at-death by quantitative methods. This device was selected only as a reference for comparing two low cost scanners and its routine use in anthropology would be too expensive and impractical.

Larger deviations between captured surfaces are more evident on more wrinkled surfaces, e.g. sample no. 390 that was obviously a very young individual (partially unfused iliac crest). Therefore, further investigation is needed to clarify whether the effect of different scanners is more obvious in more wrinkled surfaces, typical for younger individuals.

Conclusion

The two tested scanning technologies, structured light and laser represented by HP 3D SLS and NextEngine, respectively did show only small surface deviation from the reference sample in our study. The structured light technology seems to be more accurate (captures slightly more details) than laser technology. Nevertheless, no significant impact on age and sex estimates was observed. Except for TPS/BE model in age estimation. Thus, it appears that the type of scanner does not have a significant effect on the estimate of the biological profile under optimal scanning settings. However, we encourage further investigation especially in case of age-at-death estimation, where even subtle changes to the articulation surface are evaluated. Both, existing as well as future analyses of these surfaces could be sensitive to their different 3D representations acquired with different devices.

Acknowledgments

We would like to thank the Department of Anthropology at the National Museum in Prague for providing the osteological material.

This research has been supported by the research grant Charles University Grant Agency No. 642218 and partially by IRN Bipedal Equilibrium, CNRS, France.

References

[1] C. Villa, J. Buckberry, N. Lynnerup, Evaluating osteological ageing from digital data, J. Anat. (2016). https://doi:10.1111/joa.12544.

[2] M. Friess, Calvarial shape variation among Middle Pleistocene hominins: An application of surface scanning in paleoanthropology, CR Palevol. 9 (2010) 435–443. https://doi:10.1016/j.crpv.2010.07.016.

[3] S.C. Kuzminsky, M.S. Gardiner, Three-dimensional laser scanning : potential uses for museum conservation and scientific research, J. Archaeol. Sci. 39 (2012) 2744–2751. https://doi:10.1016/j.jas.2012.04.020.

[4] M. Friess, Scratching the surface? The use of surface scanning in physical and paleoanthropology, J. Anthropol. Sci. 90 (2012) 1–25. https://doi:10.4436/jass.90004.

[5] T.J.U. Thompson, P. Norris, A new method for the recovery and evidential comparison of footwear impressions using 3D structured light scanning, Sci. Justice. 58 (2018) 237–243. https://doi:10.1016/j.scijus.2018.02.001.

[6] S. Naether, U. Buck, B. Raess, M. Thali, Crime scene reconstruction using 3-D scanning and medical imaging technologies, Sci. Justice. 50 (2010) 35. https://doi:10.1016/j.scijus.2009.11.037.

[7] A. Slizewski, M. Friess, P. Semal, Surface scanning of anthropological specimens: nominal-actual comparison with low cost laser scanner and high end fringe light projection surface scanning systems, Quartär. 57 (2010) 179–187.

[8] D. Viggiano, T. Thanassoulas, C. Di-Cesare, G. Cacciola, N.M. Giorgio, T. Pitsios, C. Passiatore, A low-cost system to acquire 3D surface data from anatomical samples, Eur. J. Anat. 19 (2015) 343–349.

[9] S.C. Aung, R.C.K. Ngim, S.T. Lee, Evaluation of the laser scanner as a surface measuring tool and its accuracy compared with direct facial anthropometric measurements, Br. J. Plast. Surg. 48 (1995) 551–558. https://doi:10.1016/0007-1226(95)90043-8.

[10] M. Cantín, M. Muñoz, S. Olate, Generation of 3D Tooth Models Based on Three-dimensional Scanning to Study the Morphology of Permanent Teeth, Int. J. Morphol. 33 (2015) 782–787.

[11] D. Gibelli, V. Pucciarelli, P. Poppa, M. Cummaudo, C. Dolci, C. Cattaneo, C. Sforza, Three-dimensional facial anatomy evaluation: Reliability of laser scanner consecutive scans procedure in comparison with stereophotogrammetry, J. Craniomaxillofac. Surg. 46 (2018) 1807–1813. https://doi:10.1016/j.jcms.2018.07.008.

[12] J.W. Adams, A. Olah, M.R. McCurry, S. Potze, B.A. Wilson, Surface model and tomographic archive of fossil primate and other mammal holotype and paratype specimens of the ditsong national museum of natural History, Pretoria, South Africa, PLoS One. 10 (2015) 1–14. https://doi.org/10.1371/journal.pone.0139800

[13] S.P. Mcpherron, T. Gernat, J. Hublin, Structured light scanning for high-resolution documentation of in situ archaeological finds, J. Archaeol. Sci. 36 (2009) 19–24. https://doi:10.1016/j.jas.2008.06.028.

[14] M. Guydish, K. Henson, Using digitized Native American skeletal remains to conduct osteological analyses, Proc. W. Va. Acad. Sci. 89 (2017).

[15] A. Mathys, J. Brecko, P. Semal, Comparing 3D digitizing technologies: What are the differences?, *Digital Heritage International Congress (DigitalHeritage),* IEEE, (2013) 201–204.

[16] M.T. Ferreira, A.H. Ross, E. Cunha, A reflection on the maintenance of identified skeletal collections state of preservation, Rev. Med. Leg. 8 (2017) 186. https://doi.org/10.1016/j.medleg.2017.10.017

[17] D. Errickson, I. Grueso, S.J. Griffith, J.M. Setchell, T.J.U. Thompson, C.E.L. Thompson, R.L. Gowland, Towards a Best Practice for the Use of Active Non-contact Surface Scanning to Record Human Skeletal Remains from Archaeological Contexts, Int. J. Osteoarchaeol. 27 (2017) 650–661. https://doi:10.1002/oa.2587.

[18] S. Klein, M. Avery, G. Adams, S. Pollard, S. Simske, From scan to print: 3D printing as a means for replication, in: NIP & Digital fabrication conference. Society for imagining science and technology. (2014) 417–421.

[19] R.M. Carew, R.M. Morgan, C. Rando, A Preliminary Investigation into the Accuracy of 3D Modeling and 3D Printing in Forensic Anthropology Evidence Reconstruction, J. Forensic Sci. 64 (2018) 342–352. https://doi:10.1111/1556-4029.13917.

[20] R.J. Chase, G. LaPorte, The Next Generation of Crime Tools and Challenges: 3D Printing, National Institute of Justice. 279 (2017) 49–57.

[21] R. Rmoutilová, P. Guyomarc'h, P. Velemínský, A. Šefčáková, M. Samsel, F. Santos, B. Maureille, J. Brůžek, Virtual reconstruction of the Upper Palaeolithic skull from Zlatý Kůň, Czech Republic: Sex assessment and morphological affinity, PLoS One. 13 (2018) e0201431.

[22] G. Weber, K. Schäfer, H. Prossinger, P. Gunz, P. Mittereocker, H. Seidler, Virtual anthropology: the digital evolution in anthropological sciences, J. Physiol. Anthropol. Appl. Human Sci. 20 (2001) 69–80.

[23] S. Benazzi, G. Gruppioni, D.S. Strait, J.J. Hublin, Technical Note: Virtual reconstruction of KNM-ER 1813 Homo habilis cranium, Am. J. Phys. Anthropol. 153 (2014) 154–160. https://doi:10.1002/ajpa.22376.

[24] N. Langley-Shirley, M.A. Tersigni-Tarrant, Forensic Anthropology A Comprehensive Introduction, second ed., CRC Press, Boca Raton, 2017.

[25] E. Nikita, Osteoarchaeology: A guide to the macroscopic study of human skeletal remains, Academic Press, London, 2017.

[26] S. Mestekova, J. Bruzek, J. Veleminska, K. Chaumoitre, A Test of the DSP Sexing Method on CT Images from a Modern French Sample, J. Forensic Sci. 60 (2015) 1295–1299. https://doi:10.1111/1556-4029.12817.

[27] T. Chapman, P. Lefevre, P. Semal, F. Moiseev, V. Sholukha, S. Louryan, M. Rooze, S. Van Sint, Sex determination using the Probabilistic Sex Diagnosis (DSP : Diagnose Sexuelle Probabiliste) tool in a virtual environment, Forensic Sci. Int. 234 (2014) 189-e1. https://doi:10.1016/j.forsciint.2013.10.037.

[28] M.J. Citardi, B. Herrmann, C.S. Hollenbeak, B.C. Stack, M. Cooper, R.D. Bucholz, Comparison of scientific calipers and computed-enabled CT review for the measurement of skull base and craniomaxillofacial dimensions, Skull Base. 11 (2001) 5–11. https://doi:10.1055/s-2001-12781

[29] L. Corron, F. Marchal, S. Condemi, K. Chaumoître, P. Adalian, Evaluating the Consistency, Repeatability, and Reproducibility of Osteometric Data on Dry Bone Surfaces, Scanned Dry Bone Surfaces, and Scanned Bone Surfaces Obtained from Living Individuals, BMSAP. 29 (2017) 33–53. https://doi:10.1007/s13219-016-0172-7.

[30] M.A. Verhoff, F. Ramsthaler, J. Krähahn, U. Deml, R.J. Gille, S. Grabherr, M.J. Thali, K. Kreutz, Digital forensic osteology-Possibilities in cooperation with the Virtopsy®project, Forensic Sci. Int. 174 (2008) 152–156. https://doi:10.1016/j.forsciint.2007.03.017.

[31] R.A. Mullins, J. Albanese, Estimating Biological Characteristics With Virtual Laser Data, J. Forensic Sci. 63 (2018) 815–823. https://doi:10.1111/1556-4029.13621.

[32] B. Musilová, J. Dupej, J. Velemínská, K. Chaumoitre, Exocranial surfaces for sex assessment of the human cranium, Forensic Sci. Int. 269 (2016) 70–77. https://doi:10.1016/j.forsciint.2016.11.006.

[33] E.E. Abdel Fatah, N.R. Shirley, R.L. Jantz, M.R. Mahfouz, Improving sex estimation from crania using a novel three-dimensional quantitative method, J. Forensic Sci. 59 (2014) 590–600. https://doi:10.1111/1556-4029.12379.

[34] O. Bulut, A. Petaros, I. Hizliol, S.K.T.S. Wärmländer, B. Hekimoglu, Sexual dimorphism in frontal bone roundness quantified by a novel 3D-based and landmark-free method, Forensic Sci. Int. 261 (2016) 162.e1-162.e5. https://doi:10.1016/j.forsciint.2016.01.028.

[35] E. Cavaignac, K. Li, M. Faruch, F. Savall, P. Chiron, W. Huang, N. Telmon, Three-dimensional geometric morphometric analysis reveals ethnic dimorphism in the shape of the femur, J. Exp. Othopaedics. 4 (2017) 13. https://doi:10.1186/s40634-017-0088-2.

[36] R.E. Murphy, H.M. Garvin, A Morphometric Outline Analysis of Ancestry and Sex Differences in Cranial Shape, J. Forensic Sci. 63 (2018) 1001–1009. https://doi:10.1111/1556-4029.13699.

[37] C. Villa, J. Buckberry, C. Cattaneo, B. Frohlich, N. Lynnerup, Quantitative analysis of the morphological changes of the pubic symphyseal face and the auricular surface and implications for age at death estimation, J. Forensic Sci. 60 (2015) 556–565. https://doi.org/10.1111/1556-4029.12689.

[38] D.E. Slice, B.F.B. Algee-Hewitt, Modeling Bone Surface Morphology: A Fully Quantitative Method for Age-at-Death Estimation Using the Pubic Symphysis, J. Forensic Sci. 60 (2015) 835–843. https://doi.org/10.1111/1556-4029.12778.

[39] D. Stoyanova, B.F.B. Algee-Hewitt, D.E. Slice, An enhanced computational method for age-at-death estimation based on the pubic symphysis using 3D laser scans and thin plate splines, Am. J. Phys. Anthropol. 158 (2015) 431–440. https://doi.org/10.1002/ajpa.22797.

[40] D.K. Stoyanova, B.F.B. Algee-Hewitt, J. Kim, D.E. Slice, A Computational Framework for Age-at-Death Estimation from the Skeleton: Surface and Outline Analysis of 3D Laser Scans of the Adult Pubic Symphysis, J Forensic Sci. 62 (2017) 1434–1444. https://doi.org/10.1111/1556-4029.13439.

[41] M. San-Millán, C. Rissech, D. Turbón, Shape variability of the adult human acetabulum and acetabular fossa related to sex and age by geometric morphometrics. Implications for adult age estimation, Forensic Sci. Int. 272 (2017) 50–63. https://doi.org/10.1016/j.forsciint.2017.01.005.

[42] C. Villa, D. Gaudio, C. Cattaneo, J. Buckberry, A.S. Wilson, N. Lynnerup, Surface Curvature of Pelvic Joints from Three Laser Scanners: Separating Anatomy from Measurement Error, J. Forensic Sci. 60 (2015) 374–381. https://doi.org/10.1111/1556-4029.12696.

[43] L. Poláček, Das Hinterland des frühmitelalterlichen Zentrums in Mikulčice. Stand und Perspektiven der Forschung, in: L. Poláček (Ed.), Das Wirtschäftliche Hinterl. Der Frühmittelalterlichen Zentren. Int. Tagungen Mikulčice VI, Archeologický ústav Akademie věd ČR, Brno, 2008: pp. 257–298.

[44] D.H. Nawabi, N.A. Nassif, H.T. Do, K. Stoner, M. Elpers, E.P. Su, T. Wright, H.G. Potter, D.E. Padgett, What Causes Unexplained Pain in Patients With Metal-on metal Hip Devices? A Retrieval, Histologic, and Imaging Analysis, Clin. Orthop. Relat. Res. 472 (2014) 543–554. https://doi:10.1007/s11999-013-3199-9.

[45] R.B. Cook, N.R. Shearwood-Porter, J.M. Latham, R.J.K. Wood, Volumetric assessment of material loss from retrieved cemented metal hip replacement stems, Tribiology Int. 89 (2015) 105–108. https://doi:10.1016/j.triboint.2014.12.026.

[46] ACC SILICONES LTD. *Technical Data Sheet* [online], (2017). https://acc-silicones.com/products/moulding_rubbers/MM242R

[47] M. Tuke, A. Taylor, A. Roques, C. Maul, 3D linear and volumetric wear measurement on artificial hip joints-Validation of a new methodology, Precis. Eng. 34 (2010) 777–783. https://doi.org/10.1016/j.precisioneng.2010.06.001.

[48] The MathWorks, Inc. *MATLAB R2015b* [software], (2015).

[49] P. Cignoni, M. Callieri, M. Corsini, M. Dellepiane, F. Ganovelli, G. Ranzuglia, MeshLab: an Open-Source Mesh Processing Tool, 6th *Eurographics Italian chapter conference*. (2008) 129–136.

[50] GOM GmbH. *GOM Inspect 2016* [software], (2016).

[51] P. Murail, J. Bruzek, F. Houët, E. Cunha, DSP: A tool for probabilistic sex diagnosis using worldwide variability in hip-bone measurements, BMSAP. 17 (2005) 167–176.

[52] J. Brůžek, F. Santos, B. Dutailly, P. Murail, E. Cunha, Validation and reliability of the sex estimation of the human os coxae using freely available DSP2 software for bioarchaeology and forensic anthropology, Am. J. Phys. Anthropol. 164 (2017) 440–449. https://doi:10.1002/ajpa.23282.

[53] Morphome3cs II, CGG MFF UK, (2015). http://www.morphome3cs.com/.

[54] N. Lottering, M.S. Reynolds, D.M. MacGregor, M. Meredith, L.S. Gregory, Morphometric modelling of ageing in the human pubic symphysis: Sexual dimorphism in an Australian population, Forensic Sci. Int. 236 (2014) 195.e1-e11. https://doi.org/10.1016/j.forsciint.2013.12.041.

[55] S. Stomfai, W. Ahrens, K. Bammann, É. Kovács, S. Marild, N. Michels, L. Moreno, H. Pohlabeln, A. Siani, M. Tornaritis, T. Veidebaum, D. Molnár, Intra- and inter-observer reliability in anthropometric measurements in children, Int. J. Obes. 35 (2011) 45–51. https://doi:10.1038/ijo.2011.34.

[56] M.P.S. Machado, S.T. Costa, A.R. Freire, D. Navega, E. Cunha, E. Daruge Júnior, F.B. Prado, A.C. Rossi, Application and validation of Diagnose Sexuelle Probabiliste V2 tool in a

miscegenated population, Forensic Sci. Int. 290 (2018) 351.e1-351.e5. https://doi:10.1016/j.forsciint.2018.06.043.

[57] R.M. Carew, D. Errickson, Imaging in forensic science : Five years on, J. Forensic Radiol. Imaging. 16 (2019) 24–33. https://doi:10.1016/j.jofri.2019.01.002.

[58] G. Quatrehomme, I. Radoman, L. Nogueira, P. du Jardin, V. Alunni, Sex determination using the DSP (probabilistic sex diagnosis) method on the coxal bone: Efficiency of method according to number of available variables, Forensic Sci. Int. 272 (2017) 190–193. https://doi:10.1016/j.forsciint.2016.10.020.

[59] A. Rodriguez Paz, J. Banner, C. Villa, Validity of the probabilistic sex diagnosis method (DSP) on 3D CT-scans from modern Danish population, Rev. Med. Leg. (2018). https://doi:10.1016/j.medleg.2018.08.002.

[60] J. Kim, B.F.B. Algee-Hewitt, D.K. Stoyanova, C. Figueroa-Soto, D. Slice, Testing Reliability of the Computational Age-At-Death Estimation Methods between Five Observers Using Three-Dimensional Image Data of the Pubic Symphysis, J. Forensic Sci. 64 (2018) 507–518. https://doi:10.1111/1556-4029.13842.

[61] A. Kotěrová, J. Velemínská, E. Cunha, J. Brůžek, A validation study of the Stoyanova et al. method (2017) for age-at-death estimation quantifying the 3D pubic symphyseal surface of adult males of European populations, Int. J. Legal Med. 133 (2018) 603–612. https://doi:10.1007/s00414-018-1934-1.

[62] B.F.B. Algee-Hewitt, A.D. Wheat, The reality of virtual anthropology: Comparing digitizer and laser scan data collection methods for the quantitative assessment of the cranium, Am. J. Phys. Anthropol. 160 (2016) 148–155. https://doi:10.1002/ajpa.22932.

[63] E. Gualdi-Russo, L. Zaccagni, V. Russo, Giovanni Battista Morgagni: facial reconstruction by virtual anthropology, Forensic Sci. Med. Pathol. 11 (2015) 222–227. https://doi:10.1007/s12024-015-9665-9.

[64] B.M. Shearer, S.B. Sholts, H.M. Garvin, S.K.T.S. Wärmländer, Sexual dimorphism in human browridge volume measured from 3D models of dry crania: A new digital morphometrics approach, Forensic Sci. Int. 222 (2012) e1–400. e5. https://doi:10.1016/j.forsciint.2012.06.013.

[65] P.S. Tambusso, H.G. Mcdonald, R.A. Fariña, Description of the stylohyal bone of a giant sloth (Lestodon armatus), Palaeontol. Electron. 18 (2015) 1–10. https://doi.org/10.26879/506.

[66] M. Maté-González, J. Aramendi, D. González-Aguilera, J. Yravedra, Statistical Comparison between Low-Cost Methods for 3D Characterization of Cut-Marks on Bones, Remote Sens. 9 (2017) 873. https://doi:10.3390/rs9090873.

[67] J. Edwards, T. Rogers, The Accuracy and Applicability of 3D Modeling and Printing Blunt Force Cranial Injuries, J. Forensic Sci. (2017) 1–9. https://doi:10.1111/1556-4029.13627.

[68] J. Viciano, S. López-Lázaro, Á. Pérez-Fernández, A. Amores-Ampuero, R. D'Anastasio, J.M. Jiménez-Triguero, Scheuermann's disease in a juvenile male from the late Roman necropolis of Torrenueva (3rd-4th century CE, Granada, Spain), Int. J. Paleopathol. 18 (2017) 26–37. https://doi.org/10.1016/j.ijpp.2017.04.003.

[69] S.T. Porter, M. Roussel, M. Soressi, A Simple Photogrammetry Rig for the Reliable Creation of 3D Artifact Models in the Field: Lithic Examples from the Early Upper Paleolithic Sequence of

Les Cottés (France), Adv. Archaeol. Pract. 4 (2016) 71–86. https://doi.org/10.7183/2326-3768.4.1.71.

[70] M. Massinon, B. Dumont, N. De Cock, S.O.T. Salah, F. Lebeau, Study of retention variability on an early growth stage herbaceous plant using a 3D virtual spraying model, Crop Prot. 78 (2015) 63–71. https://doi.org/10.1016/j.cropro.2015.08.018.

[71] J.J. Secher, T.A. Darvann, E.M. Pinholt, Accuracy and reproducibility of the DAVID SLS-2 scanner in three-dimensional facial imaging, J. Craniomaxillofac. Surg. 45 (2017) 1662–1670. https://doi.org/10.1016/j.jcms.2017.07.006

[72] J. Yravedra, J. Aramendi, M.Á. Maté-González, L.A. Courtenay, D. González-Aguilera, Differentiating percussion pits and carnivore tooth pits using 3D reconstructions and geometric morphometrics, PLoS One. 13 (2018) e0194324. https://doi.org/10.1371/journal.pone.0194324.

[73] N. Zaimovic-Uzunovic, S. Lemes, Influences of Surface Parameters On Laser 3D Scanning, IMEKO Conference Proceedings: International Symposium on Measurement and Quality Control (2010).

[74] A. Veneziano, F. Landi, A. Profico, Surface smoothing, decimation, and their effects on 3D biological specimens, Am. J. Phys. Anthropol. 166 (2018) 473–480. https://doi:10.1002/ajpa.23431.

[75] S.B. Sholts, S.K.T.S. Wärmländer, L.M. Flores, K.W.P. Miller, P.L. Walker, Variation in the measurement of cranial volume and surface area using 3d laser scanning technology, J. Forensic Sci. 55 (2010) 871–876. https://doi:10.1111/j.1556-4029.2010.01380.x.

[76] R. Singh, B. Baby, A. Suri, S. Anand, Comparison of laser and structured light scanning techniques for neurosurgery applications, 3rd International Conference on Signal Processing and Integrated Networks (SPIN), IEEE, (2016) 301–305. https://doi:10.1109/SPIN.2016.7566708.

[77] L. Camison, M. Bykowski, W.W. Lee, J.C. Carlson, J. Roosenboom, J.A. Goldstein, J.E. Losee, S.M. Weinberg, Validation of the Vectra H1 portable three-dimensional photogrammetry system for facial imaging, Int. J. Oral Maxillofac. Surg. 47 (2018) 403–410. https://doi:10.1016/j.ijom.2017.08.008.

Fig. 1 Symphyseal cast of sample no. 390

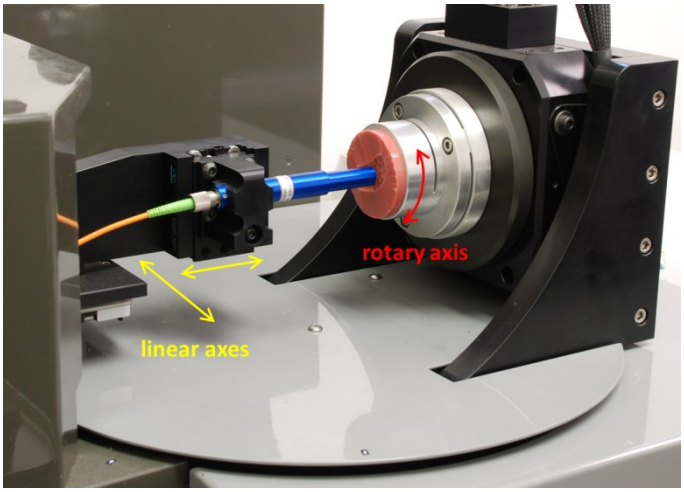

Fig. 2 Arrangement of the RedLux measuring device.

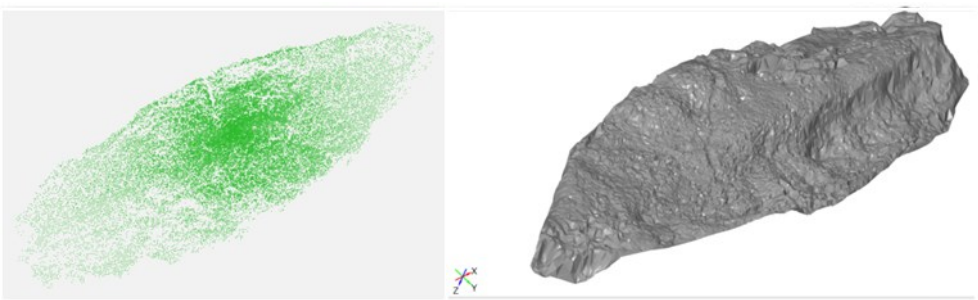

Fig. 3 left: Cloud of points (left), Mesh representation of surface (right), sample no. 359

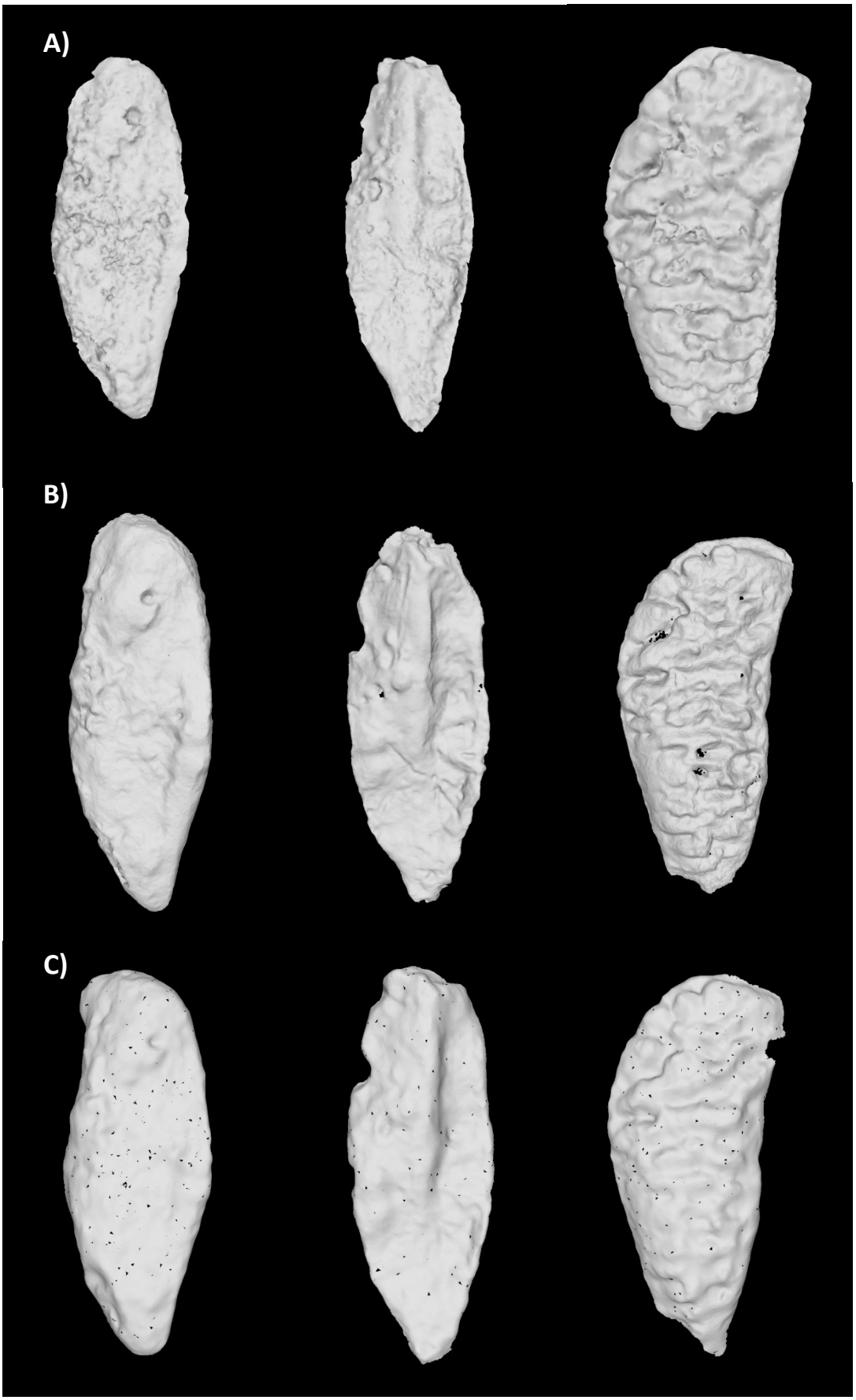

Fig. 4 Examples of digitized surfaces of isolated pubic symphyses. Models derived from RedLux (upper row), HP 3D SLS (middle row) and NextEngine (lower row).

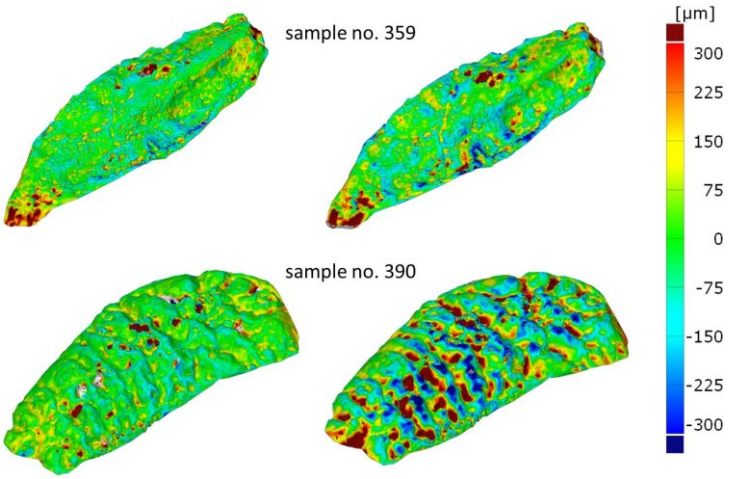

Fig. 5 Color-coded maps of the resulting deviations (sample no. 359 and 390), left: HP 3D SLS vs. reference surface, right: NextEngine laser scanner vs. reference surface.

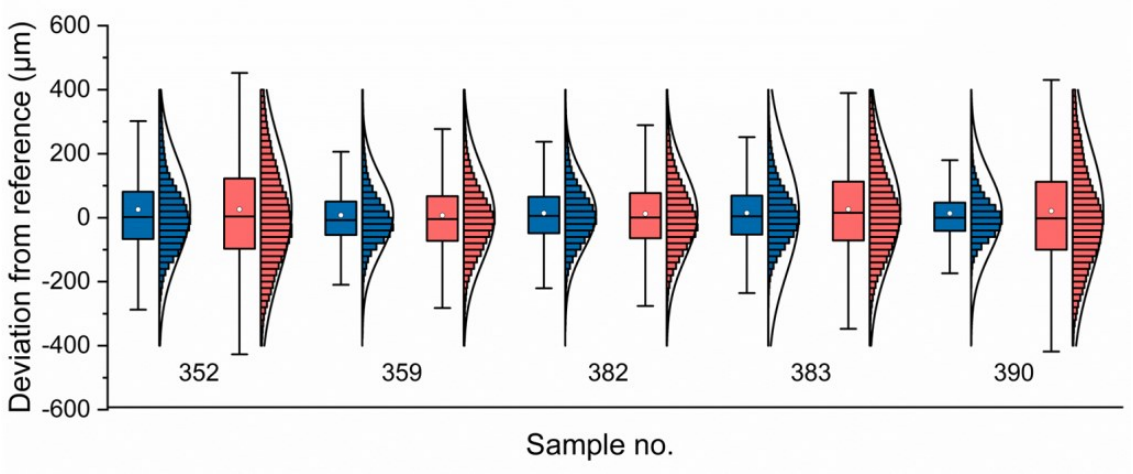

Fig. 6 Deviation from the reference sample (Redlux scan) for the HP 3D SLS (blue) and NextEngine laser scanner (red). On each box, the central mark is the median, the white point is the mean value for normal distribution μ, the edges of the box are the 25th and 75th percentiles, the whiskers extend to the most extreme data points not considered outliers.

Table 1. Os coxae measurements in DSP2.

	Variable	Name	Reference
1	**PUM**	Acetabulo-symphyseal pubic length	(Novotný 1986)
2	**SPU**	Cotylo-pubic width	(Gaillard 1960)
3	**DCOX (M1)**	Coxal length	(Braüer 1988)
4	**IIMT (M15.1)**	Greater sciatic notch height	(Braüer 1988)
5	**ISMM**	Ischium post-acetabular length	(Schulter-Ellis et al. 1983)
6	**SCOX (12)**	Iliac or coxal breadth	(Braüer 1988)
7	**SS**	Spino-sciatic length	(Gaillard 1960)
8	**SA**	Spino-auricular length	(Gaillard 1960)
9	**SIS (M14.1)**	Cotylo-sciatic breadth	(Braüer 1988)
10	**VEAC (M22)**	Vertical acetabular diameter	(Braüer 1988)

Table 2. Results of quantitative comparison between measured samples (HP 3D SLS vs. Reference sample* and NextEngine vs. Reference sample).

Specimen	Scanner	Mean value for normal distribution	Median	Standard deviation	Interquartile span	Percentage difference *IQR*
352	**HP 3D**	26	2	154	147	+50
	NextE	26	4	204	220	
359	**HP 3D**	8	-8	118	104	+35
	NextE	7	-4	146	140	
382	**HP 3D**	14	6	113	114	+24
	NextE	13	0	138	141	
383	**HP 3D**	15	5	187	122	+51
	NextE	26	15	174	184	
390	**HP 3D**	14	0	126	88	+141
	NextE	21	2	202	212	

*Reference samples were acquired by the RedLux Profiler.

Table 3. Agreement between researchers in estimating sex with the use of DSP on dry bones. Shaded cells correspond to the number of individuals in which the two researchers agreed.

		Researcher 1			
		Male	**Female**	**N/A**	**Total**
Researcher 2	**Male**	15	0	0	15
	Female	0	13	0	13
	N/A	1	0	0	1
	Total	16	13	0	29

Table 4. Agreement between researchers in estimating sex with the use of the DSP on virtual models from HP 3D SLS. Shaded cells correspond to the number of individuals in which the two researchers agreed.

		Researcher 1			
		Male	**Female**	**N/A**	**Total**
Researcher 2	**Male**	15	1	0	16
	Female	0	11	0	11
	N/A	0	1	1	2
	Total	15	13	1	29

Table 5. Agreement between two researchers in estimating sex with the use of the DSP on virtual models from NextEngine. Shaded cells correspond to the number of individuals in which the two researchers agreed.

		Researcher 1			
		Male	**Female**	**N/A**	**Total**
Researcher 2	**Male**	15	0	0	15
	Female	0	12	0	12
	N/A	1	0	1	2
	Total	16	12	1	29

Table 6. The intra-observer precision of measured variables used for DSP.

	Researcher 1						Researcher 2					
	dry bones		HP 3D SLS		NextEngine		dry bones		HP 3D SLS		NextEngine	
Variable	TEM	*r*TEM	TEM	*r*TEM	TEM	*r*TEM	TEM	*r*TEM	TEM	*r*TEM	TEM	*r*TEM
PUM	1.19	1.58	1.24	1.64	1.38	1.84	0.56	0.74	0.82	1.07	1.17	1.51
SPU	0.89	3.09	0.80	2.85	0.67	2.36	0.56	1.97	0.63	2.22	0.46	1.57
DCOX	0.77	0.35	0.49	0.23	1.11	0.51	0.45	0.20	0.83	0.38	1.19	0.55
IIMT	1.35	2.91	0.91	2.05	0.78	1.76	0.94	2.07	0.88	2.02	0.85	1.95
ISMM	1.25	1.14	0.57	0.52	1.31	1.16	0.47	0.43	0.67	0.60	0.55	0.49
SCOX	0.57	0.35	0.35	0.21	0.33	0.20	0.55	0.34	0.30	0.19	0.12	0.07
SS	0.43	0.57	0.43	0.58	0.26	0.35	0.60	0.81	0.24	0.33	0.47	0.63
SA	0.68	0.84	0.53	0.67	0.40	0.50	1.01	1.25	0.38	0.48	0.42	0.52
SIS	0.32	0.80	0.40	1.03	0.38	0.97	0.49	1.24	0.43	1.11	0.26	0.66
VEAC	0.54	0.95	0.52	0.91	0.58	1.00	0.60	1.07	0.45	0.81	0.24	0.43
mean	0.80		0.62		0.72		0.62		0.56		0.57	

TEM = technical error of measurement, *r*TEM = relative technical error of measurement, the measurement unit of TEM is given in mm, *r*TEM expressed as a percentage

Table 7. Results of measurement differences (used for the sex estimation with the DSP) on dry bones, 3D models made with HP 3D SLS and NextEngine between two researchers.

Variable	N	Max difference (mm)	Mean difference (mm)	SD	p-value
Dry bones					
PUM	29	4.00	1.22	4.99	0.05
SPU	28	4.00	1.34	3.06	0.11
DCOX	27	4.00	0.98	9.18	0.53
IIMT	28	4.50	1.79	6.79	<0.005
ISMM	29	3.50	1.07	5.98	<0.001
SCOX	15	3.00	0.83	6.27	0.01
SS	28	3.50	1.70	3.64	<0.001
SA	28	4.50	1.70	4.34	0.12
SIS	29	2.00	0.45	2.9	0.27
VEAC	29	3.50	0.97	2.99	0.02
HP 3D SLS					
PUM	29	5.00	1.66	4.88	0.18
SPU	28	3.30	1.04	3.01	0.22
DCOX	27	6.49	2.18	8.49	0.21
IIMT	28	5.24	1.79	6.86	0.02
ISMM	29	5.00	1.01	5.99	<0.01
SCOX	15	3.81	1.11	6.49	0.04
SS	28	3.32	0.96	3.66	<0.001
SA	28	4.10	0.97	4.61	0.89
SIS	29	1.01	0.51	2.93	<0.01
VEAC	29	4.97	1.90	3.07	<0.001
NextEngine					
PUM	29	7.76	2.51	4.63	<0.001
SPU	28	3.49	1.16	3.14	0.07
DCOX	27	7.46	2.13	9.25	0.01
IIMT	28	4.88	1.49	7.08	0.22
ISMM	29	2.60	0.82	6.21	0.83
SCOX	15	5.18	0.97	6.60	0.20
SS	28	2.85	1.19	3.67	<0.001
SA	28	3.01	0.98	4.68	0.51
SIS	29	2.09	0.54	2.75	0.44
VEAC	29	4.31	2.39	3.32	<0.001

Table 8. Results of a paired t-test between the estimated ages based on models from HP 3D SLS and NextEngine.

Regression model	p-value
TPS/BE[1]	0.01
SAH[2]	0.07
VC[3]	0.10
TPS/BE+VC[4]	0.27
SAH+VC[5]	0.41

[1] Thin plate spline/Bending energy, [2] Slice and Algee-Hewitt score, [3] Ventral curvature, [4] combination of TPS/BE and VC (multivariate model), [5] combination of SAH score and VC (multivariate model) P-values are shown for a two-tailed test.

Table 9. Results of a paired t-test for differences between estimated ages derived from the HP 3D SLS vs RedLux and between NextEngine vs RedLux

	HP 3D SLS vs. RedLux	NextEngine vs. Redlux
Regression model	**p-value**	
TPS/BE[1]	0.74	0.41
SAH[2]	0.04	0.03
VC[3]	0.30	0.18
TPS/BE+VC[4]	0.87	0.99
SAH+VC[5]	0.05	0.03

[1] Thin plate spline/Bending energy, [2] Slice and Algee-Hewitt score, [3] Ventral curvature, [4] combination of TPS/BE and VC (multivariate model), [5] combination of SAH score and VC (multivariate model) P-values are shown for a two-tailed test.